**Queries for apls-65-12-01**

**This manuscript/text has been typeset from the submitted material. Please check this proof carefully to make sure there have been no font conversion errors or inadvertent formatting errors. Allen Press.**

# Near-Infrared (NIR) Interactance System for Non-contact Monitoring of the Temperature Profile of Baked Liver Pâté

**MARION O'FARRELL,* KARI ANNE HESTNES BAKKE, JON TSCHUDI, and JENS PETTER WOLD**

*Sintef ICT, Forskningsveien 1, 0373, Oslo, Norway (M.O., K.A.H.B., J.T.); and Nofima Mat AS, Osloveien 1, 1430 Ås, Norway (J.P.W.)*

**This article investigates the possibility of using non-contact interactance as a method for profiling the temperature in a processed meat product (liver pâté) as it comes out of the oven. The application was defined by an industrial partner, Nortura SA, Tønsberg, Norway, where more control of the cooking process was desired. The optical system employs low spectral resolution to achieve high enough signal-to-noise ratio (SNR) to depths of 2 cm into the product. The partial least squares (PLS) method was applied to interactance spectra in the region 760-1040 nm and a root mean square error of 1.52 °C was obtained. The model was tested on five different validation sets spread over 18 months and a root mean square error of prediction of 2.66 °C was achieved. The output of this model was based on the weighted average of two temperatures in the first 2 cm of the liver pâté, one of which is the core temperature. A comparison was also made with two other models: a model based on the core temperature alone and a model based again on the weighted temperature but using the shorter wavelength range of 905.5–1047 nm. These two models gave less favorable prediction errors.**

Index Headings: **Near-infrared spectroscopy; NIR spectroscopy; Partial least squares; PLS; Nondestructive testing; Nondestructive measurements; Non-contact optics; Interactance; Temperature measurements; Water; Food; Quality control.**

## INTRODUCTION

Core temperature is a critical control parameter used in the monitoring of cooked, ready-to-eat products in terms of cooking loss, food safety, and energy efficiency. Typical current practice involves random product sampling followed by thermocouple insertion, which incurs large batch losses if an incorrect temperature level is read. This error can easily be up to 6 °C for complex products, thus requiring that food is overcooked to ensure that everything is cooked. While contact measurements of temperature are accepted in the food industry, there is a desire for non-contact, nondestructive temperature measurements, in real-time, for improved control of the cooking process.

Current non-contact temperature measurement systems are based on infrared (IR) radiation, in which the thermal radiation is emitted from an object in the range from short to long wave infrared, typically 1.4–100 μm. The amount of radiation emitted by an object is dependent on its temperature and emissivity, i.e., the ratio of energy emitted from an object to that of a black body at the same temperature.[1] From an industrial point of view IR radiation imaging is most commonly used in applications such as checking mechanical equipment for hot spots or for monitoring or controlling oven or refrigeration temperatures. FLIR Systems, for example, is involved in the development of infrared imaging technology specifically for food safety inspection to check that foods are stored at the correct temperature. The FLIR ThermaCAM is used for inspecting the electrical and mechanical equipment found in food retail, warehousing, and production facilities. By monitoring power loss in food storage and production areas, potential increases in storage temperatures can be avoided.

While infrared imaging is applied in some food processes for non-contact temperature measurements,[2] it is restricted in terms of penetration depth, i.e., it only measures the surface temperature, therefore not allowing direct measurement of the hazardous critical control point (HACCP), the core temperature. There has been research in the area of correlating the surface temperature measured by an infrared camera to the core temperature of food using algorithms based on modeling the heat transfer of the food in the regions 3.4–5 $\mu m^3$ and 8–14 μm.[4] In the paper by Stewart et al.,[4] a case study was conducted in which a Mikron 7302 micro-bolometer camera was placed at the exit of an oven at Gold Kist, Boaz, Alabama, to monitor the surface temperature based on radiation and calculate the core temperature based on the rate of surface cooling over a 75 cm distance. This installation was investigated over one year with changeover between chicken nuggets and chicken patties. Calibrations were performed at three and six months to check stability of the system and there was no significant drift over the period. The algorithm development for such surface to core temperature calculation is certainly an issue and it is often the case that black box solutions such as neural networks are employed to deal with the complexity.[3] Despite the potential of thermal imaging in terms of belt coverage and automation possibilities, it is still not widely applied in the food industry and process lines continue to employ technicians to perform the task.

Screening the temperature in food can be done by monitoring the spectral properties of the water peak in the near-infrared (NIR) region. This is no longer an emission measurement; instead the spectral changes occur due to reflected/transmitted radiation. Water has absorption peaks at 840 nm, 970 nm, 1190 nm, 1450 nm, and 1940 nm due to a combination of the third overtone of the OH stretching band and the OH bending, the second overtone of the OH stretching band, the combination of the first overtone of the OH stretching and the OH bending band, the first overtone of the OH stretching band, and combination of the OH stretching band and the OH bending band, respectively.[5,6] Most applications that monitor temperature effect on the water peak are interested in the correction of NIR-based calibration models (partial least squares (PLS), for example) for temperature effects.[7–10] There have also been studies on verifying the endpoint temperature (EPT) of heat-treated food.[11,12] In EPT estimation, the NIR measurement is taken after heat treatment and subsequent

Received 23 February 2011; accepted 6 September 2011.
* Author to whom correspondence should be sent. E-mail: marion.ofarrell@sintef.no.
DOI: 10.1366/11-06277


0003-7028/11/6512-000000$2.00/0

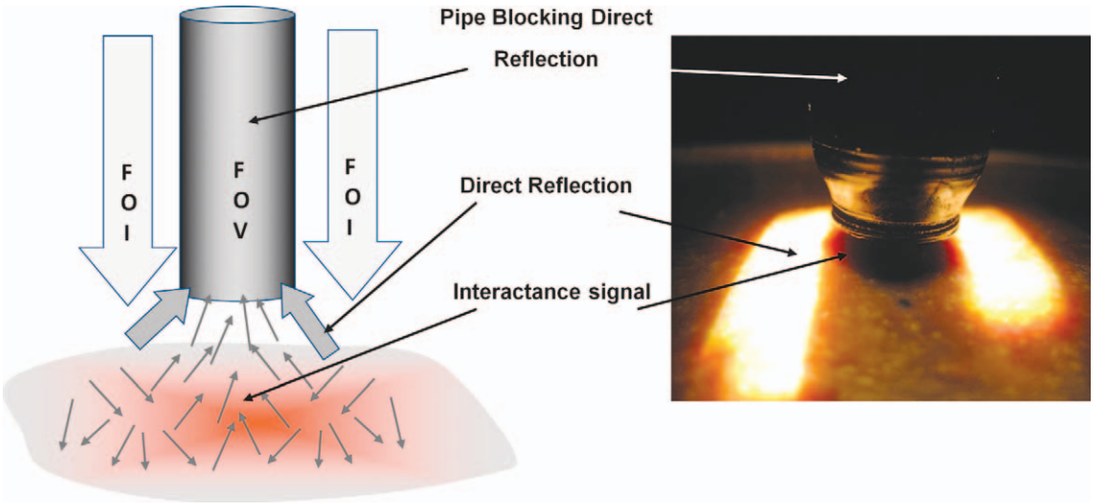


FIG. 1. Non-contact interactance in liver pâté. Samples are presented just below the pipe.

chilling, not during heat treatment. The wavelength range used is 1100–2500 nm and the spectral changes seen are mostly due to denaturation of the proteins combined with changes in the state of water.

Using the water peaks in the NIR has been investigated for noninvasive tissue temperature measurements in the medical industry.[13,14] As pointed out in these articles, there are considerations to be made when measuring water in tissue (or food) as it is dependent on both temperature and water state or binding.[13] Water binding refers to whether the water is free or bound. Water molecules can be bound to other water molecules through hydrogen bonding because the molecule is polar. It is also possible that water is bound to other molecules in the tissue/food, such as protein, and this also affects the spectral shape. Increasing temperature causes a decrease in the hydrogen bonding, causing the peak to narrow and shift towards shorter wavelengths. The presence of other molecules, on the other hand, increases hydrogen bonding, causing the peak to broaden and shift towards longer wavelengths. Therefore, these two effects are competing against each other simultaneously. In general, the higher the water content, the greater the amount of free water and the more similar the water peak is to pure water. The effect of bound water in food is discussed in an article[15] in which the water peak at 1400 nm in sliced pear was examined as the slice was dehydrated. It was found that as the percentage of bound water increased during dehydration, the water peak decreased at 1406 nm and increased at 1430 nm, i.e., there was a shift to longer wavelengths.

There are several challenges when using NIR for measuring the core temperature of food. First there is the problem of light penetration. Higher NIR wavelengths are strongly absorbed by water over short distances, and thus penetration of light is limited, which can affect direct measurements of core temperature. This can be improved by using shorter wavelengths below 1100 nm. The wavelength range discussed in this article is 760 nm to 1040 nm. When looking at temperature-induced spectral effects on liver-based product such as pâté, one would expect a change in the water peaks at 840 nm and 970 nm and a change in the myoglobin-related peak at 760 nm.[16,17] Scattering of light is also an issue as multiple light scattering can obscure temperature-dependant spectral shifts. This is a hindering factor in the measurements of tissue temperature and it increases with depth of penetration.[13,14]

The objective of this paper was to evaluate the possibility of using the wavelength range 760-1040 nm for rapid and non-contact determination of temperature development in baked portions of liver pâté at the exit of an industrial conveyor belt oven. The measurements were done with a novel NIR based system that allows rather deep penetration of light, giving optical sampling that is representative of the temperature within the samples. Measurements were done on several batches of baked pâtés over time to validate the accuracy and robustness of the method.

## MATERIALS AND METHODS

**Near-Infrared Interactance System.** Previous research in the area of fat and pigment measurements in live salmon resulted in the development of an NIR measurement system that eliminates surface reflection and resolves the interacted light into visible (Vis) and NIR spectra, each with a 20 nm resolution (460–740 nm and 760-1040 nm).[18] During the core temperature investigation, the NIR region was used, with focus on the second overtone of water at 970 nm. By using the shorter NIR wavelength range, the absorbance from water is less, allowing the light to travel further into the sample. This, combined with the low spectral resolution of the specially designed spectrometer, results in a signal-to-noise ratio (SNR) of 250 for a 15 ms spectral reading from pâté. The measurement setup is shown in Fig. 1. The system is calibrated by using a barium sulfate trough with a curved base. It is held under the pipe allowing light to pass from the field of illumination (FOI) to the field of view (FOV). The time of each measurement was one second.

The infinite thickness, or the depth at which deeper layers no longer affect the measurements for the pâté, was determined by placing a 4 cm layer of pâté on top of a highly reflective material and gradually slicing layers off while recording the spectra. This was repeated on a black absorbing material and the point at which the spectra from these two setups deviate

**TABLE I. The batches of pâté that were cooked for the experiment.**

| Group Name | Date | Initial T ( °C) | Number of NIR measurements | Core temperature range ( °C) | Duration in oven after initial T reached |
|---|---|---|---|---|---|
| Test set 1 (TS1) | April 09 | 40 | 9 (9 containers) | 86.1–101.3 | 20 minutes |
| Test set 2 (TS2) | April 09 | 3, 13, 40 | 17 (17 containers) | 76–99.8 | 50 minutes |
| Calibration Set (CS) | Oct 09 | 40 | 68 (34 containers) | 70–100.4 | 1hr 30mins |
| Test set 3 (TS3) | Oct 09 | 40 | 66 (33 containers) | 71–100.9 | 1hr 37mins |
| Test set 4 (TS4) | Oct 10 | 40 | 62 (31 containers) | 74.7–100.4 | 2hrs 4mins |
| Test set 5 (TS5) | Oct 10 | 40 | 72 (36 containers) | 75.4–100.4 | 1hr 25mins |

was taken to be the infinite thickness. In the case of pâté, this was determined to be approximately 2 cm.

**Materials and Calibration Strategy.** Three sets of experiments were conducted over 18 months in which six batches of pâté were delivered frozen from Nortura SA, Tønsberg, Norway, and allowed to defrost overnight in a fridge at 4 °C before the experiments began. The pâtés were brought to an initial equalized temperature of 40 °C before baking, as done in industry (there was one exception, where one set was brought to various initial temperatures as a test on the model). The pâté were then baked to core temperatures ranging between 71 °C and 101.3 °C in an Electrolux MENU/9764531201 convection oven (Electrolux, Stockholm, Sweden). The difference in temperature between the pâtés was achieved by different cooking time for the pâtés constituting each batch. The pâtés were removed from the oven one by one and measured immediately. They were kept intact in their alumina containers during measurements.

First, rapid (1 second) NIR measurements were taken at two positions, at the center and halfway between the center and end as one looks down on the pâté. These two readings are regarded as separate measurements throughout the experiment. Then the temperature at 1.5 cm down (core) and 0.5 cm down was recorded with a K2 type thermocouple at the same two positions on the pâté.

One of the Oct 09 batches, consisting of a total of 68 NIR measurements on 34 containers of pâté, was used as a calibration set and the other five batches were used as validation sets. The six batches are described in Table I. In the two sets from April (TS1 and TS2) NIR measurements were taken at the center position only and they were used to test samples with (1) an initial temperature of 40 °C that were cooked at a faster rate, creating a darker crust with different scattering properties and potentially different temperature gradients (TS1), and (2) samples that were cooked with three different initial core temperatures, 3 °C, 13 °C, and 40 °C, to achieve an exaggerated temperature variation in the product. These were also cooked at a fast rate (TS2). Although this temperature variation would not be found in a realistic processing plant, it gives a good indication of the robustness of the model and how deep into the product the temperature was actually measured. TS3 was taken on the day of the calibration set and TS4 and TS5 were used to test the robustness of the model by repeating the test a year after the calibration data was collected. The temperature profile of each reading was defined as the temperature difference between the depths 0.5 cm and 1.5 cm. The validation sets were cooked for various lengths of time to give good variation in terms of the temperature profile. This was done to test the limits of the model and demonstrate that the spectral information was representative of the temperature of the pâté.

**Spectral Preprocessing and Modeling.** The spectra were processed as follows to minimize scattering effects:

(1) Linearization of the spectra using the log of the inverse of the interactance spectrum ($\log(1/T)$);
(2) Standard normal variate (SNV) applied to $\log(1/T)$.

Partial least squares regression (PLSR) was applied to the calibration data set to obtain a calibration model. Full cross-validation was applied to determine the optimal number of PLS factors and to evaluate the model's predictive ability. The prediction error was estimated by the root mean square error of cross-validation (RMSECV):

$$RMSECV = \sqrt{\frac{1}{N}\sum_{i=1}^{N}(y_i - \hat{y}_i)^2} \quad (1)$$

where $\hat{y}_i$ is the predicted temperature from the cross-validation, $y_i$ is the measured reference temperature, and $i$ denotes the samples from 1 to $N$.

The performance of the different models during the industrial testing was evaluated by studying the root mean square error of prediction (RMSEP), which is calculated exactly as the RMSECV.

Calibration development was done by the software package Unscrambler 9.8 (Camo Software AS, Oslo, Norway), while all operations on the spectra were performed with Matlab version 7.9.0.529 (R2009b) (The Mathworks Inc., Natick, MA).

## RESULTS AND DISCUSSION

**Spectral Interpretation.** Figure 3 shows spectra of both water and pâté measured using the NIR system. The water measurement was set up so that light from the source was transmitted through 4 cm of boiling water and reflected back up

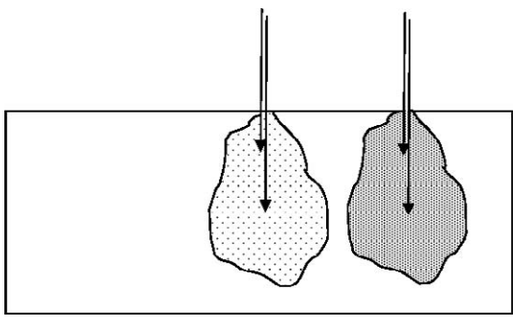

FIG. 2. Side view of pâté. NIR measurements were taken at two positions for each pâté. Shaded areas indicate the area in which the light interacts with the pâté. Arrows mark the two temperature measurements at 0.5 cm and 1.5 cm down for each position.

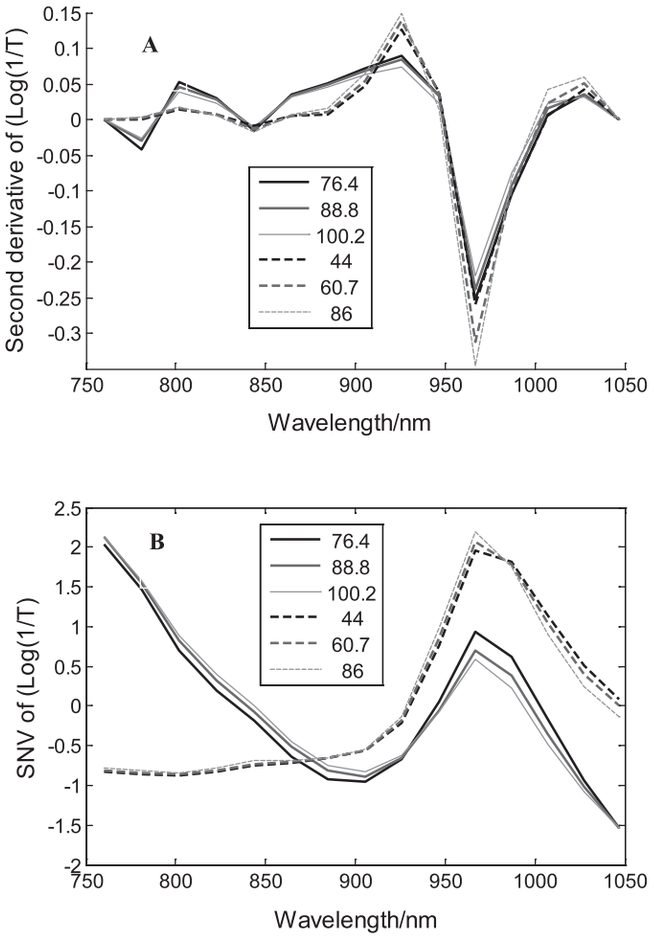


FIG. 3. (**A**) Second derivative of log (1/*T*) and (**B**) SNV of log (1/*T*) of both water (dashed traces) and pâté (solid traces) at various temperatures (°**C**).

to the field of view using the barium sulfate reference trough. Spectral and temperature measurements were taken at intervals as the water cooled. Figure 3A shows the second derivative of the log (1/*T*). There are two distinctive negative peaks in both the water and pâté derivative spectra at 840 nm and 970 nm and these are the water peaks described above. The pâté has another negative peak at 780 nm, where the water has none. This is most likely related to the myoglobin peak at 760 nm, which would be quite high in concentration in liver, the main ingredient of the pâté. The main ingredients are porcine liver (36%), pork cheek meat (26%), skimmed milk, and porcine meat (5%). This peak would be seen more clearly in the second derivative if the spectrum continued to shorter wavelengths. The myoglobin absorption peak is, however, very clear in Fig. 3B, where the SNV spectrum shows a large absorption peak around 760 nm. Figure 3B also clearly shows the narrowing of the water peak and shifting to shorter wavelengths that occurs as the water is heated and the hydrogen bonds between water are broken. This is not as obvious in pâté but it is still evident to some extent. The reason it is more difficult to see is that there exists a counteracting broadening and high wavelength shift due to hydrogen binding between water and other molecules in the pâté mixture. It is also due to the fact that the percentage of hydrogen bound water is higher since there is reduction of free water molecules caused by the dehydration during baking (the mixture enters the oven as a liquid batter and comes out firm and solid).

**Calibration Modeling.** The spectra from the calibration set taken in October 2009 were used for the models. Three models were built based on the SNV applied to log (1/*T*). The first model was based on the full spectrum from 760 to 1047 nm. The second model was based on the water peak alone from 905.5 to 1047 nm. The outputs of both of these models were based on a weighted average (30:70) of the temperature measurements taken 1.5 cm down (core) and 0.5 cm down, respectively. This weighing was done to take into account that the temperature profiles of the pâté can vary. The temperature profile of each reading is defined as the temperature difference between the 0.5 cm and 1.5 cm down (core) readings and is shown in Fig. 4. Using the weighted average also imitates the light interaction with the pâté: it is assumed, with the setup used for these experiments, that the majority of the light comes from the upper layers of the pâté but that there is also a contribution from as far down as 2 cm into the pâté. It was also discovered that due to the aluminum foil container in which the

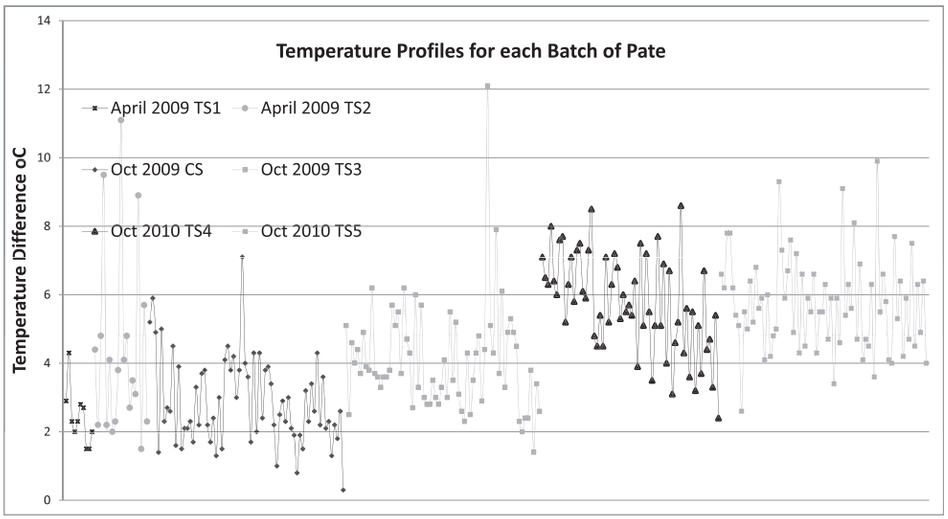


FIG. 4. Temperature profiles for each batch of pâté (temp at 1.5 cm down minus temp at 0.5 cm down).

**TABLE II. PLS calibration information.**

| Pretreatment | Wavelength range/nm | Model output | No. of PLS factors | $R^2$ | RMSECV | No. of samples | Core temp range ( °C) |
|---|---|---|---|---|---|---|---|
| Log (1/$T$) + SNV | 760–1047 (15 channels) | Weighted temp | 3 | 0.99 | 1.52 | 64 | 70–100.4 |
| Log (1/$T$) + SNV | 905.5–1047 (8 channels) | Weighted temp | 2 | 0.97 | 2.06 | 62 | 70–100.4 |
| Log (1/$T$) + SNV | 760–1047 (15 channels) | Core temp | 2 | 0.97 | 1.51 | 62 | 70–100.4 |

pâté was baked, surface evaporation caused the temperature at the core to be unexpectedly higher than that at 0.5 cm down. It was, therefore, important to include information about the lower temperature reading near the surface for food safety reasons. A third model was also investigated using only the core temperature as the output. This was done to demonstrate the advantage of using the weighted temperature as the output. The details of all of the models are given in Table II. The correlations between predicted and measured temperature were high, and the prediction errors were at a level very acceptable for process control use. Figure 5 shows the regression vectors for these models. It is clear that the regression vectors for the full spectrum models apply weight to the shift of the two water peaks 840 nm and 970 nm and the pigment peak at 760 nm.

**Validation of Models.** The three models were validated using the validation sets TS1–TS5. Figure 6 shows the predicted temperatures of all validation sets using the full spectrum model with weighted temperature as the output. The prediction details are given in Table III. TS3, TS4, and TS5 were well predicted while TS1 and TS2 had significant bias in their predictions, especially TS1. As described above, these two validation sets were the most unrealistic with regards the standard process and were used to test the limits of the model. TS1 was cooked at a very fast rate and had a darker crust than the other pâté batches and TS2 had different starting temperatures and was cooked at a fast rate, which would affect the baking development. The RMSEP of all the validation sets together in Fig. 6 is 2.66 °C. If TS1 and TS2 are removed, this is reduced to 2.38 °C.

Table III shows the prediction details for each validation set separately. If the second derivative of spectra from TS1 and TS2 (those with the largest prediction error and marked 1, 2, 3, and 4 in Fig. 6) are compared to spectra in the calibration set with similar core temperature (Fig. 7), it is clear that there is a particularly large difference at the lower wavelengths, which is probably related to the heme pigment, myoglobin. Jaywant et al.[18] did a study on bovine liver at three temperatures, 35 °C, 50 °C, and 78 °C, in which the scattering coefficient, $\mu_s'$, and absorption coefficient, $\mu_a$, were measured using an integrating sphere and structural images were taken of the samples using a transmission electron microscope. Two wavelengths were examined, 633 nm and 810 nm. The general trend for liver with heating was that the scattering particles decreased in size from 500-1000 nm to 100 nm due to coagulation, causing a faster rate of decrease in anisotropy, $g$, with increasing temperature at 633 nm than at 810 nm. This corresponds to a greater change in $\mu_s'$ at shorter wavelengths, i.e., at 633 nm than at higher wavelengths, i.e., 810 nm. It is also the case that with increasing temperature the number of scattering particles increases. These particles are arranged randomly in liver (as opposed to in a structured way in muscle), causing an almost twofold increase in $\mu_s'$ (from 25 $cm^{-1}$ to 50 $cm^{-1}$ between 50 °C and 78 °C at 810 nm). In liver, it was concluded that the continuous increase in $\mu_s'$ with increasing temperature was due to the large globulin proteins (a heterogeneous group of proteins with typical high molecular weight) that denature with temperature. This corresponds well with our data, where the validation sets TS1 and TS2 were cooked at a faster rate than the other sets, which would cause faster changes in product texture and color (Fig. 8). This in turn would lead to greater differences around the pigment absorption peak at the lower wavelengths.

Figure 9 shows the predicted temperature of all the validation sets using the water peak based model. The prediction details are given in Table IV. In this case TS1 and TS2 show an improvement in prediction because the lower wavelengths are removed, which indicates that focusing on the water peak reduces the likelihood of interfering parameters such as pigment and scattering due to pigment changes.

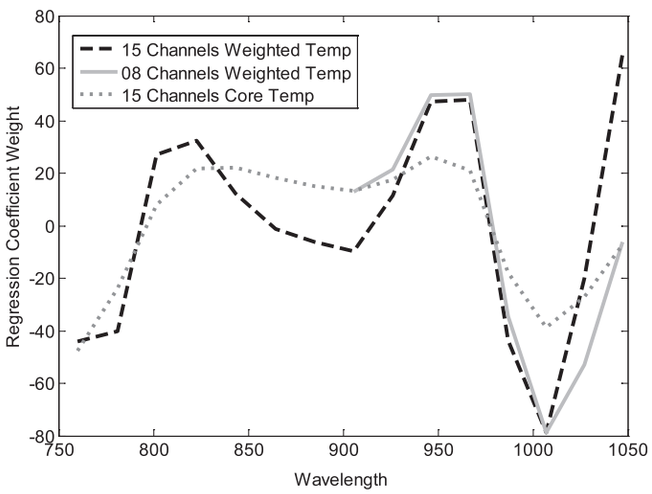


FIG. 5. Regression vectors for the three models as described in Table II.

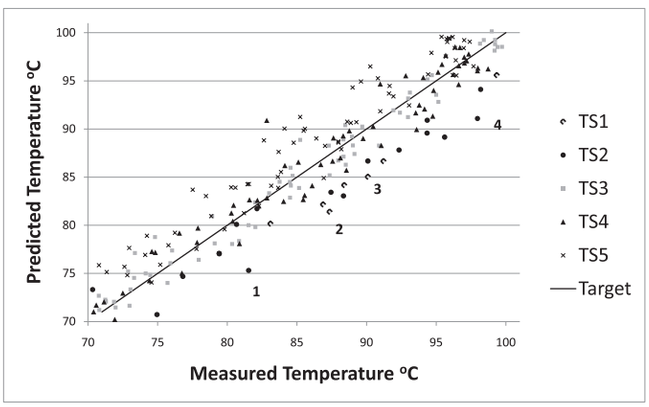


FIG. 6. Prediction of validation sets using the full spectrum model. Model output is weighted temperature. Data points marked 1–4 from TS1 and TS2 have high prediction errors.

**TABLE III. Prediction details for each validation set using model 1.**

| Set | $R^2$ | RMSEP | Bias | No. of Samples |
|---|---|---|---|---|
| TS1 | 0.43 | 4.29 | −4.19 | 9 |
| TS2 | 0.75 | 4.18 | −2.48 | 17 |
| TS3 | 0.97 | 1.53 | −0.02 | 66 |
| TS4 | 0.97 | 2.00 | 0.07 | 62 |
| TS5 | 0.97 | 3.19 | 2.49 | 72 |

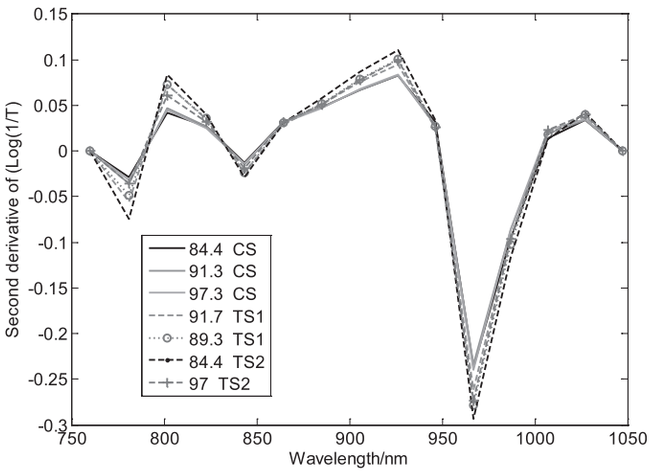


FIG. 7. Second derivative spectra from TS1 and TS2 compared with CS. The legend shows the core temperature and batch name. The spectra from TS1 and TS2 are those marked 1–4 in Fig. 6.

However, a surprising outcome of this result is the large offset that exists between TS4 and TS5. These validation sets were taken on the same day from the same delivery from Nortura and their temperature profiles were very similar (Fig. 4). The temperature measurements were also taken by the same person for both batches so human error is less likely. The biggest difference between the two batches was that TS4 was in the oven longer and was therefore cooked at a slower rate. This model is based entirely on the water peak, which is shown in Fig. 10 for various samples from TS4 and TS5. It is clear that the water peak spectra from TS4 are broader than those from TS5. In fact, the difference between the two spectra at approximately 85 °C is almost as big as the difference between the two spectra at 88.8 °C and 76.4 °C in Fig. 3. It is possible that this occurs, not due to temperature differences but due to the counteracting increasing hydrogen bonding that occurs with increasing dehydration, which is masking the temperature effect. This increased dehydration in TS4 could be caused by the longer duration in the oven. The TS4 spectrum at 85.4 °C was from a pâté sample that was 1hr in the oven and the TS5 spectrum at 84.4 °C was one that was only 30 minutes in the oven. By focusing on the water peak alone in the model, the output is more susceptible to this interfering parameter than if the entire spectrum is used.

Figure 11 shows the predictions of the third model for the two validations sets, with the biggest difference in temperature profile from the calibration set, using just core temperature as the output of the model. The prediction details are given in Table V. TS3 and TS5 both have larger temperature profiles than the calibration set. The calibration set has an average temperature profile of 2.87 °C, whereas TS3 and TS5 are 4.08 °C and 5.74 °C, respectively. The fact that the temperature distribution is not uniform in the depths where the light is traveling is clearly evident from the bias that appears in the predictions of these validation sets (Table V). The samples are nearly all under-predicted. These predictions demonstrate the need to take into account the temperature profile in the model. They also demonstrate how modeling the temperature based on surface IR radiation could give inaccuracies based on variations in the temperature profiles.

## CONCLUSION

Results presented here demonstrate an online, non-contact method for monitoring the temperature profile of liver pâté as it exits the oven. The NIR system is based on remote interactance measurements in the short wave NIR region 760-1040 nm.

Three models were tested, one with the full spectral range including the two water peaks and the pigment peak (output: weighted temperature), one with just the main water peak at 970 nm (output: weighted temperature), and a third with the full spectral range including the two water peaks and the pigment peak (output: core temperature). It was found that by using the 970 nm water peak alone, the model was more susceptible to the hydration levels of the product but was more robust against pigment variation. By using the full spectrum, differences in hydration levels had less of an influence. However, the validation sets with greater pigment deviations from being cooked at a faster rate were poorly classified. In an industrial setting, parameters such as baking duration and oven temperature are usually less variable and the initial temperature of the product is typically equalized. This minimizes the


FIG. 8. Difference between samples that are cooked at a faster rate (0.6 °C $min^{-1}$) and slower rate (0.33 °C $min^{-1}$).

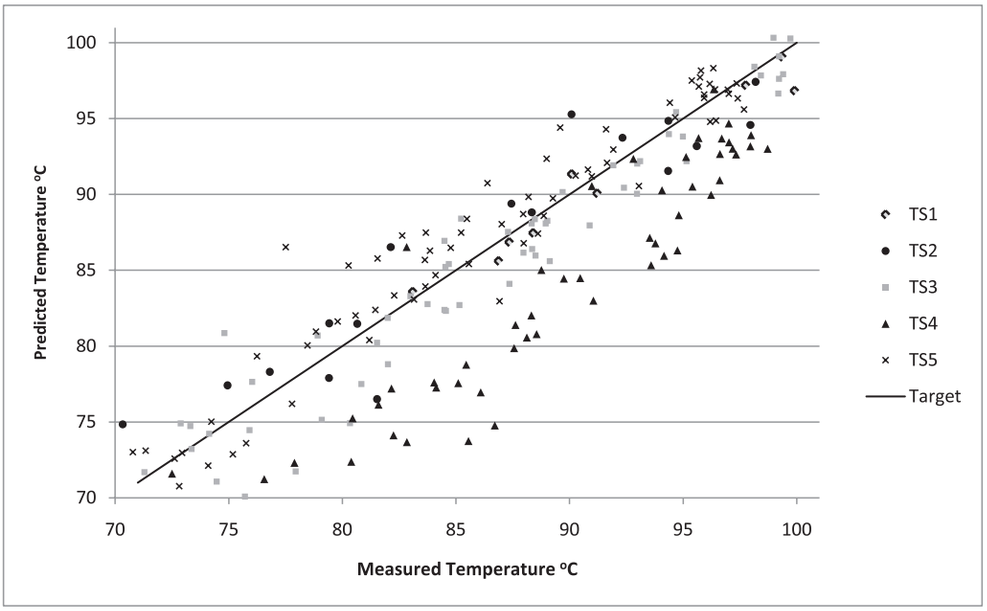


FIG. 9. Prediction of TS1–TS5 using the water peak based model. Model output is weighted temperature.

**TABLE IV. Prediction details for each validation set using model 2.**

| Set | $R^2$ | RMSEP | Bias | No. of samples |
|---|---|---|---|---|
| TS1 | 0.95 | 1.31 | −0.66 | 9 |
| TS2 | 0.88 | 2.86 | 0.56 | 17 |
| TS3 | 0.92 | 2.60 | −1.17 | 66 |
| TS4 | 0.37 | 6.85 | −6.01 | 62 |
| TS5 | 0.91 | 2.59 | 0.85 | 72 |

probability of the occurrence of such large variations in the product. It was still, however, useful to test such variations in order to check the limitations of the model. The model that was based on core temperature alone was dependent on the temperature variation in the first 2 cm of the pâté, which is not surprising since the light travels to and collects information from that depth. By using the weighted temperature, the model output was much more robust against variations in the temperature profile.

In terms of applying such a system online, it would be better practice to use a model based on the entire spectral range, thus making it less susceptible to hydration levels. Hydration would be something that is more likely to vary in a real life factory than the pigment. Occurrences such as product flow delays, storage duration of raw materials, or room temperature and humidity level, which could cause evaporation of water from the product, are more likely to occur than the oven temperature

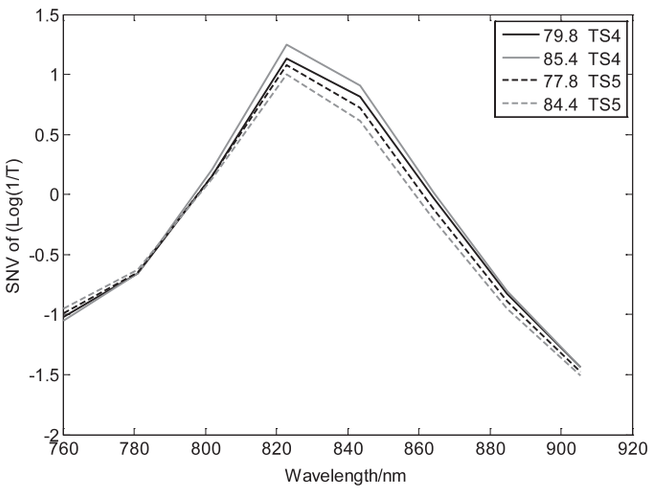


FIG. 10. Water peak of spectra from TS4 and TS5 with similar temperature profiles. The legend shows the core temperature and batch name.

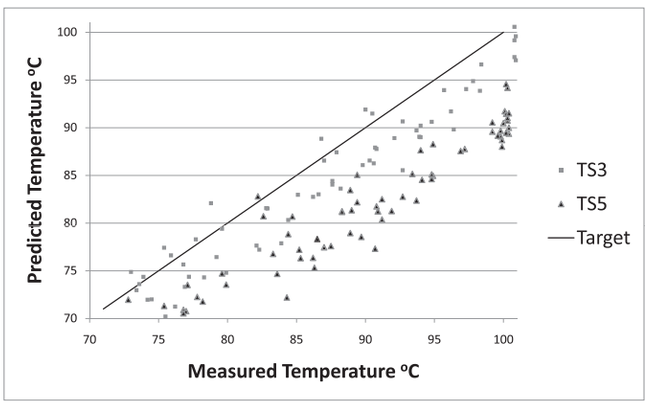


FIG. 11. Comparison of the prediction of TS3 and TS5 using a model based on the full spectrum. Model output is the core temperature alone.

**TABLE V. Prediction details for each validation set using model 3.**

| Set | $R^2$ | RMSEP | Bias | No. of samples |
|---|---|---|---|---|
| TS3 | 0.96 | 3.31 | −2.17 | 66 |
| TS5 | 0.95 | 13.79 | −13.46 | 62 |

suddenly increasing, resulting in a faster cooking rate. The RMSEP of the validation sets TS1–TS5 were 4.29 °C, 4.18 °C, 1.53 °C, 2 °**C**, and 3.19 °C, respectively, when using the full spectrum model. The RMSEP of all the data sets grouped together was 2.66 °C. If TS1 and TS2 are removed this is reduced to 2.38 °C.

The system described here offers an opportunity to monitor the temperature development of the product in real time without the need for random product selection and thermocouple probing, which is dependent on human diligence to ensure the probe reaches the center of the product and is given enough time to read the temperature. It was also the case that the pâté in these experiments were not coldest at the core but rather 0.5 cm below the surface due to surface evaporation, and this would be taken into account in the measurement with the NIR system.

**ACKNOWLEDGMENTS**

The research presented here was completed as part of a project that was funded by the Norwegian Research Council (NFR) – KMB Competitive Processing (178280/I10). The authors would like to acknowledge the financial support received by the NFR and express gratitude to the industrial collaborators, who contributed both financially and by providing facilities for the industrial trials – QVision AS and Nortura S.A., Tønsberg, Norway.

1. A. A. Gowen, B. K. Tiwari, P. J. Cullen, K. McDonnell, and C. P. O'Donnell, Trends Food Sci. Technol. **21,** 190 (2010).
2. A. M. Foster, L. P. Ketteringham, G. L. Purnell, A. Kondjoyan, M. Havet, and J. A. Evans, J. Food Eng. **76,** 19 (2006).
3. J. G. Ibarra, Y. Tao, and H. Xin, Opt. Eng. **39,** 3032 (2000).
4. J. Stewart, M. Matthews, and M. Glasco, Proc. SPIE Int. Soc. Opt. Eng. **6205,** 62050N-1 (2006).
5. W. A. P. Luck, *Structure Of Water and Aqueous Solutions,* W. A. P. Luck, Ed. (Verlag Chemie, Germany, 1974), p. 248.
6. T. Kaino, Appl. Opt. **24,** 4192 (1985).
7. J. A. Hageman, J. A. Westerhuis, and A. K. Smilde, J. Near Infrared Spectrosc. **13,** 53 (2005).
8. T. Chen and E. Martin, J. Chemom. **21,** 198 (2007).
9. H. Swierenga, F. Wulfert, O. E. de Noord, A. P. de Weijer, A. K. Smilde, and L. M. C. Buydens, Anal. Chim. Acta, **411,** 121 (2000).
10. F. Wulfert, W. T. Kok, O. E. de Noord, and A. K. Smilde, Chemom. Intell. Lab. Syst. **51,** 189 (2000).
11. M. Risberg Ellekjaer and T. Isaksson, J. Sci. Food Agric. **59,** 335 (1992).
12. M. Uddin, E. Okazaki, M. U. Ahmad, Y. A. Fukuda, and M. Tanaka, J. Food Sci. Technol. **38,** 809 (2005).
13. S. H. Chung, A. E. Cerussi, S. I. Merritt, J. Ruth, and B. J. Tromberg, Phys. Med. Biol. **55,** 3753 (2010).
14. V. S. Hollis, T. Binzoni, and D. T. Delpy, Proc. SPIE Int. Soc. Opt. Eng. **4250,** 470 (2001).
15. H. Buning-Pfaue, Food Chem. **82,** 107 (2003).
16. H. J. Swatland, Can. Inst. Food Sci. Technol. J. **22,** 390 (1989).
17. H. E. Snyder, *Proc. Meat. Industry Res. Conf.,* Am. Meat Inst. Foundation, **21** (1968).
18. A. Folkestad, J. P. Wold, K. A. Rørvik, J. Tschudi, K. H. Haugholt, K. Kolstad, and T. Mørkøre, Aquaculture, **280**(1–4)**,** 129 (2008).
19. S. Jaywant, B. Wilson, M. Patterson, L. Lilge, T. Flotte, J. Woolsey, and C. McCulloch, Proc. SPIE Int. Soc. Opt. Eng. **1882,** 218 (1993).